Kinematic studies of transport across an island wake, with application to the Canary islands.

by MATHIAS SANDULESCU[1], EMILIO HERNÁNDEZ-GARCÍA[2], CRISTÓBAL LÓPEZ[2⋆], ULRIKE FEUDEL[1]

[1] *Carl-von-Ossietzky Universität Oldenburg D-26111 Oldenburg, Germany;* [2] *Instituto Mediterráneo de Estudios Avanzados, IMEDEA (CSIC - Universitat de les Illes Balears) E-07122 Palma de Mallorca, Spain*

29 May 2006

ABSTRACT

Transport from nutrient-rich coastal upwellings is a key factor influencing biological activity in surrounding waters and even in the open ocean. The rich upwelling in the North-Western African coast is known to interact strongly with the wake of the Canary islands, giving rise to filaments and other mesoscale structures of increased productivity. Motivated by this scenario, we introduce a simplified two-dimensional kinematic flow describing the wake of an island in a stream, and study the conditions under which there is a net transport of substances across the wake. For small vorticity values in the wake, it acts as a barrier, but there is a transition when increasing vorticity so that for values appropriate to the Canary area, it entrains fluid and enhances cross-wake transport.

1 Introduction

Chaotic transport in hydrodynamic flows Aref (2003); Ottino (1989); Wiggins (1999) is a subject generating a great amount of interest both in its fundamental aspects and in its applications to industrial, laboratory, and environmental flows. A class of problems of particular relevance in the context of ocean modelling is the one of transport across jets (Bower, 1991; Samelson, 1992; Meyers, 1994; Rogerson et al., 1999; Cencini et al., 1999). One of the outcomes of these studies is that ocean jets can behave, depending on parameter regimes, both as barriers to the transport of the particles and as mixing enhancers, increasing the interchange of water masses across them Bower et al. (1985). Typically there is an increased fluid transport when enhancing the time dependence of the jet, associated to an increased chaotic behavior of the fluid trajectories.

In this Paper we consider a related issue, namely that of fluid transport across a wake. The motivation arises from situations occurring in front of the Canary upwelling zone in the Northwest African coast Arístegui et al. (1997); Barton et al. (1998, 2004); Pelegri et al. (2005) (See Fig. 1).

⋆ Corresponding author.

e-mail: clopez@imedea.uib.es

There is a strong mesoscale activity in the wake of the Canary Islands, originated from the current impinging on them from the North, and running southwards or southwestwards more or less parallel to the African coast. Wind stress in the lee region of the islands plays also a role in the generation of mesoscale eddies Arístegui et al. (1997); Barton et al. (1998). At the same time there is intense upwelling of depth nutrient-rich waters at the African coast which is produced by winds parallel to the coast via the Ekman mechanism. These two systems interact giving rise to filaments of great biological productivity and complex dynamics. Our aim in this Paper is to explore a very simple kinematic mechanism for the formation of such filaments: entrainment by the wake. We will also determine whether the wake will act as a barrier, i.e. it will stop the flux of nutrient-rich water towards the ocean interior, or rather cross-wake transport will be increased by the presence of eddies. In the second case, which is the one realized in our model for parameter values appropriate for the Canary zone, the mechanism may be important to enhance biological productivity of ocean regions relatively far from the coastal upwelling. In any case, we stress that in this work we focus on the transport of particles into and across the wake and not on the long-range transport that could drive them far apart from it.

In general, one can identify three possible mechanisms contributing to the horizontal transport from a coastal upwelling across a wake: The first one is the direct effect of Ekman pumping that transports the upwelled waters in the direction opposite to the coast. In the second one, coastal water parcels become entrained by the wake, which stretches and deforms them into filamental features until some parts reach the ocean interior. Third, coastal waters may become captured inside eddies, which can travel long distances.

All of the three mechanisms require the wake to be permeable to fluid trajectories, and chaotic advection behind the island to be strong enough to allow transverse transport across the main current. There have been studies of chaotic transport in flows modelling island wakes Miller et al. (2002), but the emphasis was not in transverse transport. Transport of coastal waters inside eddies and filaments has been observed in the Canary area Arístegui et al. (1997); Barton et al. (1998, 2004); Pelegri et al. (2005). Nevertheless few attention has been devoted to the relative importance and interplay between the first two mechanisms. With numerical solutions of the Navier-Stokes equations in two dimensions Duan and Wiggins (1997); Shariff et al. (1992), it has been shown, for the wake behind a cylinder, that an important increase of cross-wake transport occurs in the Reynolds number range $100 - 200$. The phenomenon has been studied in detail Duan and Wiggins (1997), and has been associated to topological changes in the structure of the wake, which allows lobes of fluid to be stretched into filaments that cross the wake. The similarity of this mechanism to what it is seen in the Canary area motivates our study, in which we try to identify an analogous mechanism in a geophysical setting. In particular, we will show a transition from a situation with a barrier that does not allow particles to cross the wake, and another one without barrier, where there is a net transport of matter across it. In the real ocean, phenomena such as eddy detachment and additional filamentation produced by hyperbolic regions in the neighborhood, can collaborate with the wake-crossing mechanism reported in this work to produce long-range transport. But these effects are absent in our model, and as already mentioned, we focus on the possibility of crossing the wake, i.e., in the fact that the particles visit the side of the wake opposite to the place from which they are released.

With this aim we use in this Paper a kinematic ap-

proach to analyze the interplay between the mechanisms of Ekman transport and entraining by the wake. We focus on horizontal transport on upper ocean layers by using a two-dimensional flow, and set up a model streamfunction having the qualitative features of the wake behind an island by modifying the streamfunction introduced in Jung et al. (1993); Ziemniak et al. (1994) to model the wake behind a cylinder. Parameters are chosen in such a way that the relevant geometric features (sizes, time scales, speeds, ...) are comparable with the real situation in the Canary Islands zone. We do not expect this to be an accurate model of the real ocean dynamics, but since the spatial and temporal scales are taken from observations, we expect it to capture the correct kinematics of the transport and the relative importance of the mechanisms involved.

In the following, we first discuss the properties of the velocity field used, and then characterize the amount of transport in several parameter regimes. To quantify it we define in the system an area outside the wake providing a continuous source of particles, and count how many of them are able to cross the wake for different parameter values. In our interpretation of the model as a representation of the Canary zone, the particle source area is intended to represent the upwelling water close to the African coast.

The Paper is organized as follows. In the next section we present the kinematic flow differentiating the three situations that we want to study: periodic flow, non-periodic flow and periodic flow with turbulent diffusion of the particles. Then in Section 4 we briefly comment on the dynamics of the particles. Section 5 contains the results of our work and in Section 6 we write down our conclusions.

2 An analytical model for the flow in the wake of an island

Full hydrodynamic simulations of flows in two or three spatial dimensions involve solving Navier-Stokes equations or approximations to it. In geophysical contexts, simplified turbulence closing schemes should be used to simulate the small unresolved scales. A simple alternative from which considerable insight has been gained in the past (Bower, 1991; Samelson, 1992; Meyers, 1994; Rogerson et al., 1999; Cencini et al., 1999) is to consider, in two-dimensional incompressible situations, a model streamfunction $\Psi(x, y, t)$ giving a flow qualitatively similar to the one under study. The velocity components in x- and y-direction and the equations of motion of fluid elements are:

$$\begin{aligned} \dot{x} &= v_x(x, y, t) = \frac{\partial}{\partial y}\Psi(x, y, t), \\ \dot{y} &= v_y(x, y, t) = -\frac{\partial}{\partial x}\Psi(x, y, t). \end{aligned} \tag{1}$$

We are interested in the transport perpendicular to the vortex street in the wake of an island. To keep the geometry of the island as simple as possible, we assume it to have a circular shape. Of course, this is a crude approximation to the Canary islands archipelago. However, observations report on the existence of vortex streets in the south of the islands which qualitatively can be understood as emerging from a single large obstacle. As in Arístegui et al. (1997), the island of Gran Canaria will be chosen here as the representative obstacle of the whole archipelago. Our streamfunction is based on the one introduced in Jung et al. (1993) and Ziemniak et al. (1994), but we add to it the effect of Ekman pumping from the coast originated by the effect of the northern winds on the African coast. In addition, we will also eventually consider vortex trajectories more complex than in Jung et al. (1993) and Ziemniak et al. (1994). The kinematic model by Jung et al. was originally developed to

describe the flow behind a cylinder of radius r located in the middle of a channel of width W. Satisfactory comparison was made with numerical solutions of the Navier-Stokes equation in the range of Reynolds numbers such that the velocity field is periodic in time (von Karman vortex street flow), i.e., for Re of order 100. It is remarkable that numerical simulations in Arístegui et al. (1997) show that already at Re$\approx$ 100, many orders of magnitude smaller than the true Reynolds number in the turbulent ocean, the flow around Gran Canaria given by a barotropic quasigeostrophic model reproduces some of the observed large scale features. This gives confidence to the hypothesis that the streamfunction in Jung et al. (1993) and Ziemniak et al. (1994), developed for flows in that order of Reynolds numbers, is a good starting point to model the large scale features of the island wake.

There are, however, many unrealistic features in it. Among them, the most noticeable is that the true geophysical flow is not time periodic. Another one is that it lacks of any of the small scale structures characteristic to real turbulent flows. To minimize these shortcomings, in this work we will present results for the transport across the wake of an obstacle for three different situations: In the first case we will use a streamfunction periodic in time, which is the direct extension of the model in Jung et al. (1993) but including an Ekman term. In a second case the motion of the vortices, which in the original model is rectilinear, will have a stochastic component, giving rise to a non-periodic flow. In the third case we will add a random velocity component to the particle motion in the periodic streamfunction, as a way to investigate the impact on transport of small-scale turbulent diffusion. These three situations are described in the next subsections.

2.1 Periodic flow

The spatial coordinates are chosen such that the mean flow runs along the horizontal x direction, from left to right, put the center of the cylinder at the origin of coordinates, and measure lengths in units of the cylinder radius, so that $r = 1$. Under these conditions the streamfunction, based in Jung et al. (1993), will be written as

$$\Psi(x, y, t) = f(x, y)g(x, y, t). \tag{2}$$

The first factor $f(x, y)$ ensures that the trajectories do not penetrate into the cylinder,

$$f(x, y) = 1 - e^{-a\left(\sqrt{x^2+y^2}-1\right)^2}. \tag{3}$$

There is a frictional boundary layer of width $a^{-1/2}$ on which the tangential velocity component tends linearly to zero, while the radial velocity component decreases quadratically. The cylinder surface can be considered as the union of an infinite number of parabolic fixed points.

The second factor $g(x, y, t)$ models the background flow, the vortices in the wake, and the Ekman term:

$$\begin{aligned} g(x, y, t) &= -wh_1(t)g_1(x, y, t) + wh_2(t)g_2(x, y, t) \\ &+ u_0 s(x, y)y + u_E(x - 1)\Theta(x - 1). \end{aligned} \tag{4}$$

The first two terms describe the simultaneous presence of two vortices in the wake. They are of opposite sign but their maximal vortex strengths are equal and denoted by w. They are of Gaussian shape:

$$g_i(x, y, t) = e^{-\kappa_0\left[\left(x-x_i(t)\right)^2+\alpha\left(y-y_i(t)\right)^2\right]}, i = 1, 2 \tag{5}$$

$\kappa_0^{-1/2}$ is the characteristic linear size of the vortices (the radius), and α gives the characteristic ratio between the elongation of the vortices in the x and y direction. The vortex centers move along the x direction according to

$$\begin{aligned} x_1(t) &= 1 + L\left(\tfrac{t}{T_c} \bmod 1\right), \quad y_1(t) = y_0 \\ x_2(t) &= x_1(t - T_c/2), \quad y_2(t) = -y_0, \end{aligned} \tag{6}$$

and their amplitudes are modulated by

$$\begin{aligned} h_1(t) &= \left|\sin\left(\pi\frac{t}{T_c}\right)\right| \\ h_2(t) &= h_1(t - T_c/2) \end{aligned} \tag{7}$$

Thus, vortices are created behind the cylinder with a dephasing of half a period. Each of them moves a distance L along the x direction during a time T_c, then fades out, and the process restarts.

The third term in $g(x, y, t)$ describes the background flow, a current of speed u_0 in the positive horizontal direction. The factor $s(x, y)$ introduces the shielding of this background flow behind the cylinder, allowing it to be replaced by the vortex structures. Its precise form is

$$s(x, y) = 1 - e^{-(x-1)^2/\alpha^2 - y^2}. \tag{8}$$

This shielded region is of size 1, i.e. of the size of the cylinder or island.

The last term in $g(x, y, t)$ is absent in the original streamfunction of Jung et al. Jung et al. (1993); Ziemniak et al. (1994). It models an additional velocity of constant strength u_E in the y direction acting only when the x coordinate of a particle is larger than 1, i.e. just behind the island (Θ is the Heavyside or step function, i.e. $\Theta(u) = 1$ if $u > 0$ and $\Theta(u) = 0$ if $u < 0$). This corresponds to a stream crossing the vortex street towards the negative y direction just past the cylinder. This term was introduced in order to take into account the existence of the Ekman-drift in the region of the Canary Islands which points towards the ocean interior. Plots of the streamlines of the flow without and with the Ekman-drift are shown in Figs. 2 and 3, respectively. The rectangle in the upper part is the area where a large number N of particles, initially equidistant, is repeatedly introduced at regular time intervals Δ. Their trajectories are followed by integrating the equations of motion (1) and from them the cross-wake transport is estimated (see below). This configuration aims at representing the transport of water parcels, rich in nutrients, from an upwelling region in the African coast towards the ocean interior.

2.2 Non-periodic flow

Real oceanic flows are never perfectly periodic. It is well known that structures that are perfect barriers to transport (Kolmogorov-Arnold-Moser (KAM) tori) in a periodic flow become leaky when the time-dependence is not exactly periodic Wiggins (1999), so that there is the possibility that the model defined in the previous subsection would underestimate transport. In addition, in the above presented periodic flow case, the trajectories of the vortices are rectilinear and regular which does not happen in the real case of Canary vortices. As a way to relax both limitations, we add some randomness to the vortex trajectories. Instead of moving along straight horizontal lines, $y_1(t) = y_0$, $y_2(t) = -y_0$, the vertical coordinates of the vortices move according to $y_1(t) = y_0 + \gamma\xi(t)$, and $y_2(t) = -y_1(t)$, where $\xi(t)$ is a normalized Gaussian white noise ($< \xi(t) >= 0$, $< \xi(t)\xi(t') >= \delta(t - t')$) and γ the noise strength. Using this approach the periodicity of the streamfunction is broken, and some of the characteristic features of periodic flows, such as the existence of strict barriers to transport, will not be present in this case. Again, particle trajectories starting in the upper rectangle are determined from equations (1).

2.3 Periodic flow with turbulent diffusion of the particles

For the preceding two cases, periodic and non-periodic flows, the trajectories of tracers are computed by integrating equations (1) with the given streamfunction. This streamfunction contains only large scale features and completely misses all the small scale turbulence that is characteristic to the real ocean.

A convenient way to include unresolved small scales in Lagrangian computations is to add to the velocity field experienced by the Lagrangian particle a fluctuating term representing small-scale turbulence Griffa (1996); Mariano et al. (2002). In our case,

$$\dot{\mathbf{x}}(t) = \mathbf{v}(\mathbf{x}, t) + \sqrt{2K}\eta(t). \tag{9}$$

where $\mathbf{x} = (x, y)$ and $\mathbf{v}(\mathbf{x}, t)$ is the velocity field given by Eq.(1) for the periodic flow case. This gives additional diffusion to particle trajectories. Usually the two-dimensional vector $\eta(t)$ is taken to be a Gaussian Markov process with a memory time of the order of some days Buffoni et al. (1997); Falco et al. (2000). Here, to explore the impact of irregular unresolved motions in the opposite extreme to the deterministic situation considered in the previous sections, we use for $\eta(t)$ a two-dimensional Gaussian white noise of zero mean and correlations $\langle \eta(t) \cdot \eta(t') \rangle = \delta(t - t')$. For the strength K we take $K \approx 10\ m^2 s^{-1}$, which is the effective eddy diffusivity estimated by Okubo (1971) as acting at the spatial scales of about 10 km, which are of the order of the spatial structures that begin to be missed from our streamfunction. In this case, some typical features of the periodic flow are lost, and even smooth dynamical systems structures become fuzzier. In particular, transport may occur even across perfect Lagrangian barriers.

3 Parameter estimation for the Canary zone

In this section we enumerate the relevant geophysical properties of the upper ocean levels of the Canary zone in order to be represented in the model. We extract the relevant information from references Arístegui et al. (1997); Barton et al. (1998, 2004); Pelegri et al. (2005). Although there are seasonal variations in most of the parameters, representative constant values are used here.

- A unique island is in the model. This mimics the Gran Canaria island, which seems to have most influence on the zonal mesoscale activity Arístegui et al. (1997). Its linear size is of the order of 54 km, from which we take the radius of the model cylinder to be $r = 25\ km$. This will be taken in the next Sections as the unit of length so that $r = 1$ there.

- Typically in this area the mean velocity is 0.05 m/s and in some periods of the year reaches 0.2 m/s. We take a background flow velocity of $u_0 = 0.18\ m/s$. In numerical experiments (with a large eddy viscosity) Arístegui et al. (1997) a von Karman vortex street appears when the background flow is larger than 0.1 m/s.

- Different sizes are observed for the Canary eddies, ranging from 50 to 100 kilometers, and depending on the distance to the island that generates them. In any case the mean radius of the eddies $\kappa_0^{-1/2}$ is comparable to that of the island that generates it. Thus we take $\kappa_0^{-1/2} = r$.

- Eddies are usually elliptic. Its eccentricity diminishes with the distance to the island. In our model we take $\alpha = 1$, that would represent circular vortices. But due to the part of the streamfunction representing shielding behind the cylinder, vortices are stretched and have some ellipticity.

- The rotation period of a buoy in an eddy Pelegri et al. (2005) ranges from 3 to 6 days (although increasing with time). This gives a linear velocity at their periphery (distance r from the center) of about 0.6 m/s. By equating this speed with typical values of derivatives of the streamfunction at the vortex periphery we estimate the vortex strength $w \approx 55 \times 10^3\ m^2/s$.

- The shedding of eddies, as already commented, is not perfectly periodic. Nevertheless we take a typical interval between eddy shedding events of 15 days. Thus $T_c = 30$ days.

- Some measurements of eddy velocities indicate that

they move towards the southwest at a velocity of $5-6$ kilometers per day. The typical displacement during a time T_c is thus $L = 150\ km = 6r$.

• Lifetime of the eddies is of several weeks, with some measurements reporting lifetimes of several months. Typically they remain close to the island for about one week. In the model the lifetime is the same as the period T_c, which is within the order of the magnitude of observed permanence in the wake.

• $a^{-1/2}$, the width of the cylinder boundary layer, is difficult to estimate since it is ill-defined at geophysical scales. Fortunately its value only affects motion close to the cylinder and its effect is unimportant in most of the velocity field. We take $a^{-1/2} = r$.

• The Ekman flow is originated by the wind stress $\tau = \rho_{air} c_d v^2$, where $\rho_{air} = 1.222\ kg/m^3$ is the air density, $c_d \approx 0.0013$ is the drag coefficient between water and air, and v is the wind velocity, typically in the range $[2.7, 8.7]\ m/s$. Thus the wind stress is in a range $[0.012, 0.12]\ N/m^2$. For a particular intermediate value of $v = 5\ m/s$ we have $\tau = 0.040\ N/m^2$.

The value of the Ekman speed is given by:

$$u_E = \frac{\tau}{\rho_0 f h}, \tag{10}$$

being $\rho_0 \approx 1024\ kg/m^3$ the sea water density, $f = 10^{-4}\ s^{-1}$ the Coriolis parameter at the Canary latitude, and h the depth of the Ekman layer. It ranges between $15\ m$ and $100\ m$. We take the intermediate value $h = 50\ m$, which can be justified from the expression $h = \sqrt{\frac{2A_v}{f}}$ for a vertical turbulent viscosity $A_v \approx 0.1\ m^2/s$. With these parameter values, and the values for the wind stress, the Ekman velocity u_E is in the range $[0.0023, 0.02]\ m/s$.

In the following, in addition to measure lengths in units of r, we measure time in units of T_c. With this, the non-dimensional values of the parameters to be used in the model read: $r = T_c = a = \alpha = 1$, $\kappa_0 = 1$, $L = 6$, $u_0 = 18.66$, $u_E \in [0.2, 2]$, $w = 200$. In the non-periodic case we use $\gamma = 0.5$ and $y_0 = 0.5$ (i.e. half the island radius) for the parameters of the vortex trajectories.

4 Particle dynamics in the wake

The dynamics given by Equations (1) can be interpreted as the equation of motion of a one-degree of freedom Hamiltonian system with time-dependent Hamiltonian $\Psi(x, y, t)$. In our case we have an open system, meaning that the particles start in an incoming asymptotic region, pass a region where the dynamics is time dependent, and then leave the system through an outgoing asymptotic region. While in the time-dependent region of the system, particles are trapped by the vortices and whirled around for a while. Since the velocity field is time dependent, particles can be handed from one vortex to the following one and can remain in the region close to the cylinder for a relatively long time, even though the vortices leave this region quite rapidly. In fact there are periodic and localized trajectories organizing these long scattering orbits. They constitute the backbone of the so-called *chaotic saddle*, the unstable set of trajectories never leaving the wake region (Jung et al., 1993). This structure, and particularly its stable and unstable manifolds (the lines along which particles ending at the saddle approach it, and particles close to the saddle leave it, respectively) organize important trajectory characteristics in the wake. More in detail, the stable or contracting manifold of the chaotic saddle is the set of spatial points x such that particles starting from x approach the chaotic saddle as time advances. Similarly, the unstable or stretching manifold is the set of points such that their backward-in-time evolution approaches the chaotic saddle. Stable manifolds cannot intersect with themselves and with other stable manifolds, and the same holds

for the unstable manifolds. Moreover, particle trajectories cannot cross these manifolds. However, stable and unstable manifolds can intersect each other. All these properties make them important templates organizing the particle trajectories in the system. Typically, vortex boundaries are areas of tangencies between stable and unstable manifolds. In the particular case of open flows, like the one studied in this work, the unstable manifold of the chaotic saddle is the set of points along which particles leave it, and, therefore, it is the set that is traced by a number of particles when they are launched in the system and take an long time to abandon it.

In Fig. 4 we show the stable and unstable manifolds of the chaotic saddle for two representative parameter sets. A clear change in the shape of the unstable manifold is seen when increasing the vortex strength w. The chaotic saddle itself, however, is only approached by particles starting on its stable manifold. In our configuration, and for the parameter values we use, these structures are closely packed very near the cylinder surface (see Fig. 4), in contrast with other situations studied in the literature (Jung et al., 1993; Ziemniak et al., 1994). As a consequence, for the initial conditions to be used in Sect. 5, tracked fluid particles will not intersect such manifold and they will not follow strongly chaotic recirculating orbits, but rather they will be advected downstream relatively fast. In addition they will leave the wake region along paths that are not perfectly aligned with the saddle's unstable manifold. Despite of this, we will see that the change of topology observed in Fig. 4 has global consequences in particle dynamics and that for realistic parameter values, corresponding to the right panel of Fig. 4, particles can cross the wake, and experience some stretching and dispersion.

5 Quantifying transport across the wake of an island

In this Section we report the numerical results obtained for the three different flows introduced in Section 2. Our objective is to quantify transport across a vortex street in the presence of a continuous source of particles representing the water parcels upwelling at the African coast. We model this source by placing test particles in the rectangle $0 < x < 1$ and $2.1 < y < 2.5$, i.e., above and at some distance of the cylinder (see Figs. 2 and 3). We place 200 new particles in the rectangle at regular intervals of time $\Delta = 0.01$ (in units of the flow period T_c), i.e. 20,000 new particles per period, and integrate their evolution under the flow. Particles are initially placed along four horizontal lines inside the rectangle, but this has no influence on the results described below.

Our open system is considered to be the region displayed in Figs. 2 and 3. Trajectories leaving this region are no longer integrated. The idea is that it will be impossible (for the periodic flow case) or practically impossible (for the non-periodic and turbulent cases) for the particles to return back to the region after they leave it. We count at every interval of time Δ how many particles have *crossed the wake*. There is some ambiguity in defining the transverse extent of the wake. Fortunately, as will become clear from the results presented later, the dynamics is such that particles either do not approach the central region behind the cylinder while they remain inside our region or rather they perform a rather large transverse excursion. Thus, any reasonable definition of 'crossing the wake' will give essentially the same results. In this Section we will count particles crossing the central line $y = 0$ as 'having crossed the wake', and at the end of the Section we will show that the same results are obtained if counting them when crossing $y = -1$

(see Fig. 13). Particles crossing the chosen line several times are counted only once.

Because of the presence of the Ekman term u_E, all trajectories will eventually reach arbitrarily negative y coordinates if observed sufficiently far downstream. Clearly, this can not be considered to be a wake crossing, and we restrict our computation to the region shown in Figs. 2 and 3, where the vortices remain localized and thus it is the only part of the flow in which nontrivial dynamics occurs. Given the simple structure of the flow, even when wake crossing occurs, the particles can not go very far and typically they will not leave the proximity of the wake region. In a more realistic ocean setting, additional mechanisms can occur after wake crossing that may bring particles further towards the open ocean. But wake crossing is anyway the first step needed for such long-range transport to occur.

We fix all but two of the parameters of the model indicated in the previous section, namely the strength of the vortices, w, and the Ekman pumping u_E, which are varied in a realistic range. The measure of transport across the wake is performed by counting the number of particles crossing the line $y = 0$ during each time interval Δ. A short transient after the launching of the first particles in the rectangle this quantity becomes a periodic function of time in the periodic flow case, and approximately periodic under the other two flows. To focus on average transverse transport, a quantity called N^c is computed as the ratio between the number of particles crossing $y = 0$ during 6 flow periods (after discarding an initial transient of 3 periods) and the total number of particles launched during that time (120,000 particles).

In Fig. 5 we plot N^c versus w for different values of the Ekman pumping strength u_E in the periodic flow case. The most relevant result is the absence of transport for small values of w, identifying the existence of a barrier that does not permit the entrance of particles in the wake. This barrier disappears when w crosses a critical value w_c which depends on the Ekman pumping strength u_E, $w_c = w_c(u_E)$. At a fixed value of u_E the proportion of crossing particles increases with increasing w as expected, above the critical threshold w_c. In Fig. 6 we plot the critical value w_c as a function of u_E. The value of w_c diminishes from approximately $w_c = 50$ for $u_E = 0.2$ to $w_c = 20$ for $u_E = 2$. Similarly for increasing u_E the ratio of particles crossing is significantly larger for a fixed w. Most importantly, for the typical realistic value $w = 200$ (see Sect. 3) one obtains a rather large proportion of crossing particles, N^c, independently of the value of u_E, so that one can expect that behind the Canary islands a net transport of particles from the coast to the opposite side of the island wake occurs.

Now we illustrate the transport mechanism by looking at particle distributions for the two different situations just identified. In Fig. 7 we show a snapshot of the particle positions, all of them launched at the horizontal lines in the marked rectangle at successive times. In the left panel we plot the case $w = 10$ in which the launching site is on the exterior of the barrier impeding transport across the wake. In the right panel ($w = 200$) we observe particles spreading through the wake of the island. Obviously a barrier no longer exists between the launching site and the lower parts of the wake. Transport occurs along a filament entrained into the wake that stretches the particle lines and later disperses them. The similarity of the tracers distribution with real features observed in the Canary area is remarkable (see for example Fig. 24 of Barton et al. (1998), or Fig. 1 of Arístegui et al. (2004)). This occurs despite the fact that, as advanced before, the trajectory structure in Fig. 7 is rather different from the saddle manifolds in Fig. 4. The difference

arise because the launching site for the tracer particles is rather far from the manifolds.

Thus we can conclude that the formation of vortices in the wake of the Canary Islands together with Ekman pumping make up a possible mechanism for the formation and entrainment of nutrient-rich filaments into the Canary wake, and eventually for transport of nutrients from the African coast to areas in the Atlantic beyond the islands. The effectiveness of this enrichment mechanism will depend however on how fast are the upwelled nutrients consumed by the biological populations near the coast (Pelegri et al., 2005). Note that since the size of the island (and so the width of the wake) is 50 km, the time the particles would need to cross the wake if driven only by the Ekman flow (u_E is in the range $[0.0023, 0.02]$ m/s) is between $28-250$ days. Given that the mean flow $u_0 = 0.18$ m/s transports particles out of the observation region shown in the figures (10 cylinder radii) in about 16 days, we see that no particles are able to cross the wake region behind the cylinder under the sole effect of the Ekman flow.

We now discuss the results for the other two flows considered. In Fig. 8 we show N^c versus w for different u_E in the non-periodic flow case, that is, with the random y component for the trajectories of vortex centers. The non-periodicity of the flow has been introduced to overcome strict barriers to transport that are not realistic. The results show that the effect of non-periodicity is not strong. We still observe a value w_c below which transport is extremely low, though it is non-zero now. Some particles can enter into the wake at low vortex strength $w < w_c$ due to the non-periodic nature of the flow, but their number is rather small. For higher vortex strength $w > w_c$ we observe an increasing net transport with increasing w. For a fixed u_E the critical value w_c is lower than the corresponding threshold in the periodic case. Fig. 9 shows distributions of tracers, again for $w = 10$ and $w = 200$. They share the qualitative features with the periodic case, Fig. 7, although now there is much more particle dispersion after the filament enters the wake.

The same plots for the case of particles driven by the periodic flow with turbulent diffusion are shown in Figs. 10 and 11. For small values of the Ekman pumping u_E there is again a critical vortex strength w_c such that for $w < w_c$ only minimal transverse transport is observed. In the realistic value, $u_E = 2$, a non-negligible net transport of particles is observed already for low vortex strength w, in contrast to the previous cases where below the critical value w_c transport was very low. Nevertheless there is still a sharp increase in effective transport when increasing w. Thus a remnant of the critical value w_c is still visible. In Fig. 11 the distribution of tracers is plotted for $w = 10$ and $w = 200$, as in the previous cases. As expected from the introduction of turbulent diffusion particles become randomly dispersed, but always around average paths similar to the previous cases.

The comparison among the three cases (periodic, non-periodic and turbulent) is shown in Fig. 12. Here we fix $u_E = 0$, $u_E = 1$ and $u_E = 2$, and plot N^c vs w for the different types of flows in one graph.

The smallest transverse transport, and the largest critical w_c, is always attained in the periodic flow case (which is the only case for which below w_c transverse transport is exactly zero). The smallest effective value of w_c is found for the case of particles with turbulent diffusion, and transport is also higher in this case for the smallest values of w and all u_E. At the other end of the considered range of w, i.e. going towards realistic values $w > 150$, the measured transport N^c is largest for the non-periodic flow case. The addition of

the turbulent particle diffusion slightly increases transport at large w with respect to the purely periodic case, but the difference between these two cases is not large. This indicates that turbulent diffusion, at least as modelled here, has no strong influence on transverse transport in the realistic limit of large w, while non-periodic vortex movement is more significant.

Finally we return to the question about the distance over which transport across the wake occurs by comparing N^c for different positions of the line which the tracers have to pass in order to be counted as particles that have actually crossed the wake. In Fig. 13 we compare the proportions of particles crossing the lines $y = 0$ and $y = -1$ for the periodic flow case and $u_E = 1$. Similar results are obtained for other values of u_E and for the other two flows. The ratio of particles crossing the line $y = 0$ is slightly higher, but both remain very similar over the entire range of w, meaning that the measured transport does not depend significatively on the choice of the position of the line the tracers must cross in the wake. This was in fact quite obvious from the shape of the particle distributions (Figs. 7,9 and 11).

6 Conclusions

The biological activity around the Canary Islands and in the open ocean depends crucially on the availability of nutrients. An important source of these nutrients is provided by the upwelling near the African coast. In a simple scenario, we have shown that these nutrients can be transported over long distances perpendicular to the coast due to the formation of filaments that are entrained into the Canary wake by the eddies present there. The intensity of this horizontal transport depends strongly on the vorticity content of the vortices, characterized by w, and the strength of the Ekman pumping u_E. Other parameters do not affect transverse transport so strongly, except the mean flow velocity u_0 that has the obvious effect of transporting the particles faster or slower downstream the wake, and thus decreasing or increasing, respectively, their chances to cross it. The mesoscale structure mediating the crossing – a meandering filament – is very similar to real structures observed in the Canary region.

Since our approach is kinematic, and parameters are directly obtained from observations, our conclusions do not depend on the particular mechanism producing the wake eddies, being it flow separation, wind stress curl on the lee of the islands (Arístegui et al., 1997; Barton et al., 1998), etc. The simplicity of our approach has allowed us to identify different factors which enhance or diminish transport across the wake. We have found that cross-wake transport occurs always at large enough w. Periodic flow contains transport barriers which block the transport from outside the wake if the vortex strength is below a critical threshold value. Such a sharp threshold is replaced by a crossover to low transport in the non-periodic case, or when a simple model of turbulent diffusion is considered. These last mechanisms enhance transport, but in rather different ways: While turbulent diffusion influences transport for small vortex strength, mainly below and close to the critical transport threshold, non-periodicity of the flow enhances transverse transport at high vortex strength. Our model of turbulent diffusion acts effectively only at small scales, while non-periodicity changes the flow on larger scales yielding a stronger overall effect.

Here we have considered only transport of passive tracers. To study the impact of the phenomena discussed here on the biological productivity off from the African coast, coupling to models of plankton dynamics should be performed. This remains an interesting task for the future. **Probably,**

vertical upwelling produced inside the cyclonic eddies would have to be taken into account.

Acknowledgements. We would like to thank Tamás Tél for many valuable discussions. M.S. and U.F. would like to acknowledge the financial support by the DFG grant FE 359/7-1(2003). E.H-G. and C.L. acknowledge financial support from MEC (Spain) and FEDER through project CONOCE2 (FIS2004-00953). Both groups have benefited from a MEC-DAAD joint program. C.L. is a *Ramón y Cajal* fellow of the Spanish MEC.

REFERENCES

Aref, H. 2002. The development of chaotic advection. *Phys. Fluids* **14**, 1315–1325.

Arístegui, J., Tett, P., Hernández-Guerra, A., Basterretxea, M., Montero, F., Wild, K., Sangrá, P., Hernández-Leon, S., Canton, M., García-Braun, J. A., Pacheco, M., and Barton, E. D. 1997. The influence of island-generated eddies on chlorophyll distribution: a study of mesoscale variation around Gran Canaria. *Deep Sea Research I* **44**, 71–96.

Arístegui, J., Barton, E. D., Tett, P., Montero, F., García-Muñoz, M., Basterretxea, G., Cussatlegras, A.-S., Ojeda, A. and de Armas, D. 2004. Variability in plankton community structure, metabolism, and vertical carbon fluxes along an upwelling filament (Cape Juby, NW Africa). *Progress in Oceanography* **62**, 95–113.

Barton, E. D., Arístegui, J., Tett, P., Canton, M., García-Braun, J., Montero, F., Nykjaer, L., Almeida, C., Almunia, J., Ballesteros, S., Basterretxea, G., Escánez, J., García-Weill, L., Hernández-Guerra, F., López-Laatzen, F., Moliona, R., Montero, M. F., Navarro-Pérez, E., Rodríguez, J. M., van Lenning, K., Vélez, K., and Wilda, K. 1998. The transition zone of the Canary Current upwelling region. *Progress in Oceanography* **41**, 455–504.

Barton, E. D., Arístegui, J., Tett, P., and Navarro-Pérez, E. 2004. Variability in the Canary Islands area of filament-eddy exchanges. *Progress in Oceanography* **62**, 71–94.

Bower, A. S., Rossby, H. T. and Lillibridge, J. L. 1985. The Gulf Stream – barrier or blender? . *J. Phys. Oceanogr.* **15**, 26–32.

Bower, A. S. 1991. A simple kinematic mechanism for mixing fluid parcels across a meandering jet. *J. Phys. Oceanogr.* **21**, 173–180.

Buffoni, G., Falco, P., Griffa, A. and Zambianchi, E. 1997. Dispersion processes and residence times in a semi-enclosed basin with recirculating gyres: An application to the Tyrhenian Sea. *J. Geophys. Res.* **102**, 18699–18713.

Cencini, M., Lacorata, G., Vulpiani, A. and Zambianchi, E. 1999, Mixing in a Meandering Jet: A Markovian Approximation . *J. Phys. Oceanogr.* **29**, 2578–2594.

Duan, J. and Wiggins, S. 1997. Lagrangian transport and chaos in the near wake of the flow around an obstacle: a numerical implementation of lobe dynamics. *Nonlinear Processes in Geophysics* **4**, 125–136.

Falco, P., Griffa, A., Poulain, P. M. and Zambianchi, E. 2003. Transport properties in the Adriatic Sea as deduced from drifter data. *J. Phys. Oceanogr.* **30**, 2055–2071.

Griffa, A. 1996. Applications of stochastic particle models to oceanographic problems. In: *Stochastic Modelling in Physical Oceanography*, (eds. R. J. Adler, P. Muller and B. L. Rozovskii), Birkhauser, Boston, 114–140.

Jung, C., Tél, T. and Ziemniak, E. 1993. Application of scattering chaos to particle transport in a hydrodynamical flow. *Chaos* **3**, 555–568.

Mariano, A. J., Griffa, A., Özgökmen, T. M. and Zambianchi, E. 2002. Lagrangian analysis and predictability of coastal and ocean dynamics. *J. Atm. Ocean. Tech.* **19**, 1114–1125.

Meyers, S. D. 1994. Cross-frontal mixing in a meandering jet. *J. Phys. Oceanogr.* **24**, 1641–1646.

Miller, P. D., Pratt, L. J., Helfrich, K. R., and Jones, C.K.R.T. 2002. Chaotic transport of mass and potential vorticity for an island recirculation. *J. Phys. Oceanogr.* **32**, 80–102.

Okubo, A. 1971. Oceanic diffusion diagrams. *Deep-Sea Research* **18**, 789–802.

Ottino, J. M. 1989. *The kinematics of mixing: stretching, chaos, and transport*, Cambridge Univ. Press, Cambridge.

Pelegrí, J. L., Arístegui, J., Cana, L., González-Dávila, M., Hernández-Guerra, A., Hernández-León, A., Marrero-Díaz, M. F., Montero, M. F., Sangrà, P., and Santana-Casiano, M. 2005. Coupling between the open ocean and the coastal upwelling region off northwest Africa: Water recirculation and offshore pumping of organic matter. *J. Mar. Sys.* **54**, 3–37.

Rogerson, A. M., Miller, P. D., Pratt, L. J., and Jones, C.K.R.T. 1999. Lagrangian motion and fluid exchange in a barotropic meandering jet. *J. Phys. Oceanogr.* **29**, 2635–2655.

Samelson, R. M. 1992. Fluid exchange across a meandering jet. *J. Phys. Oceanogr.* **22**, 431–440.

Shariff, K. T., Pulliam, T., and Ottino, J. 1992. A dynamical sys-

tems analysis of kinematics in the time-periodic wake of a circular cylinder. In: *Vortex Dynamics and vortex methods, Proc. AMS-SIAM Conf., Lectures in Applied Mathematics*, (eds. C. Anderson and C. Greengard), American Mathematical Society, Providence.

Wiggins, S. 1992. *Chaotic transport in dynamical systems*, Springer Verlag, New York.

Ziemniak, E., Jung, C. and Tél, T. 1994. Tracer dynamics in open hydrodynamical flows as chaotic scattering. *Physica D* **76**, 424.

FIGURE LEGENDS

Fig. 1. The Canary Islands region, with the Canary current running southwestwards parallel to the African coast, where there is an intense upwelling, and impinging on the islands.

Fig. 2. The streamlines of the flow without Ekman flow, $u_E = 0$, at vortex strength $w = 200$. Other parameters as described in Sect. 3. The box where tracers are starting is drawn just above the cylinder with coordinates $0 < x < 1$, and $2.1 < y < 2.5$. The snapshots are at $t = 0$ (top-left), $t = T_c/4$ (top-right), $t = 2T_c/4$ (bottom-left), and $t = 3T_c/4$ (bottom-right).

Fig. 3. Streamlines of the flow with Ekman flow $u_E = 2$ and other parameters, and time sequence of the snapshots, as in Figure 2.

Fig. 4. Stable (in gray) and unstable (in black) manifolds of the chaotic saddle in the wake of the cylinder, for the case of the periodic flow and $u_E = 2$. Left: Snapshot taken at time $7T_c$ for vortex strength $w = 10$. Right: Snapshot taken at time $7T_c$ for vortex strength $w = 200$. In the inset we show a zoom of the manifolds in the area close to the cylinder. Other parameters as described in Sect. 3. The chaotic saddle itself is closely packed immediately behind the cylinder surface. The unstable manifold has been plotted by releasing a large number of particles left of the cylinder and very close to it, letting the flow to transport them for a long time ($7T_c$ as already indicated) so that only the ones lasting at this time in the wake region are still there and plotted. The stable manifold is plotted in the same way but releasing the particles right of the cylinder and running the flow backwards in time.

Fig. 5. The ratio of particles crossing the wake, N^c, versus vortex strength w in the periodic flow. The different curves correspond to different values of the Ekman pumping, u_E, as indicated in the legend.

Fig. 6. The critical values of the vortex strength, w_c, versus the velocity of the Ekman pumping u_E in the periodic flow.

Fig. 7. Plot of the spatial distribution of the tracers in the wake of the island for the case of the periodic flow and $u_E = 2$. Left: Snapshot of the distribution of the tracers at time $0.39T_c$ for vortex strength $w = 10$. Right: Snapshot of the distribution of the tracers at time $0.39T_c$ for vortex strength $w = 200$.

Fig. 8. Proportion of particles crossing the wake, N^c, versus vortex strength w for the non-periodic flow. The different curves correspond to different values of the Ekman pumping, u_E, as indicated in the legend.

Fig. 9. Plot of the spatial distribution of the tracers in the wake of the island for the case of the non-periodic flow and $u_E = 2$. Left: Snapshot of the distribution of the tracers at time $0.39T_c$ for vortex strength $w = 10$. Right: Snapshot of the distribution of the tracers at time $0.39T_c$ for vortex strength $w = 200$.

Fig. 10. Proportion of particles crossing the wake, N^c, versus vortex strength w for the periodic flow with turbulent diffusion of the particles. The different curves correspond to different values of the Ekman pumping, u_E, as indicated in the legend.

Fig. 11. Plot of the spatial distribution of tracers in the wake of the island for the case of the periodic flow with turbulent diffusion and $u_E = 2$. Left: Snapshot of the distribution of the tracers at time $0.39T_c$ for vortex strength $w = 10$. Right: Snapshot of the distribution of the tracers at time $0.39T_c$ for vortex strength $w = 200$.

Fig. 12. Comparison of transport across the wake for

the three kinds of flows. The values of u_E and the type of flow that originated the data are indicated in the plot.

Fig. 13. N^c versus w for $u_E = 1$ for the periodic flow, and two situations: circles correspond to the proportion of particles that cross the line $y = 0$, and squares to $y = -1$. No remarkable differences can be observed.

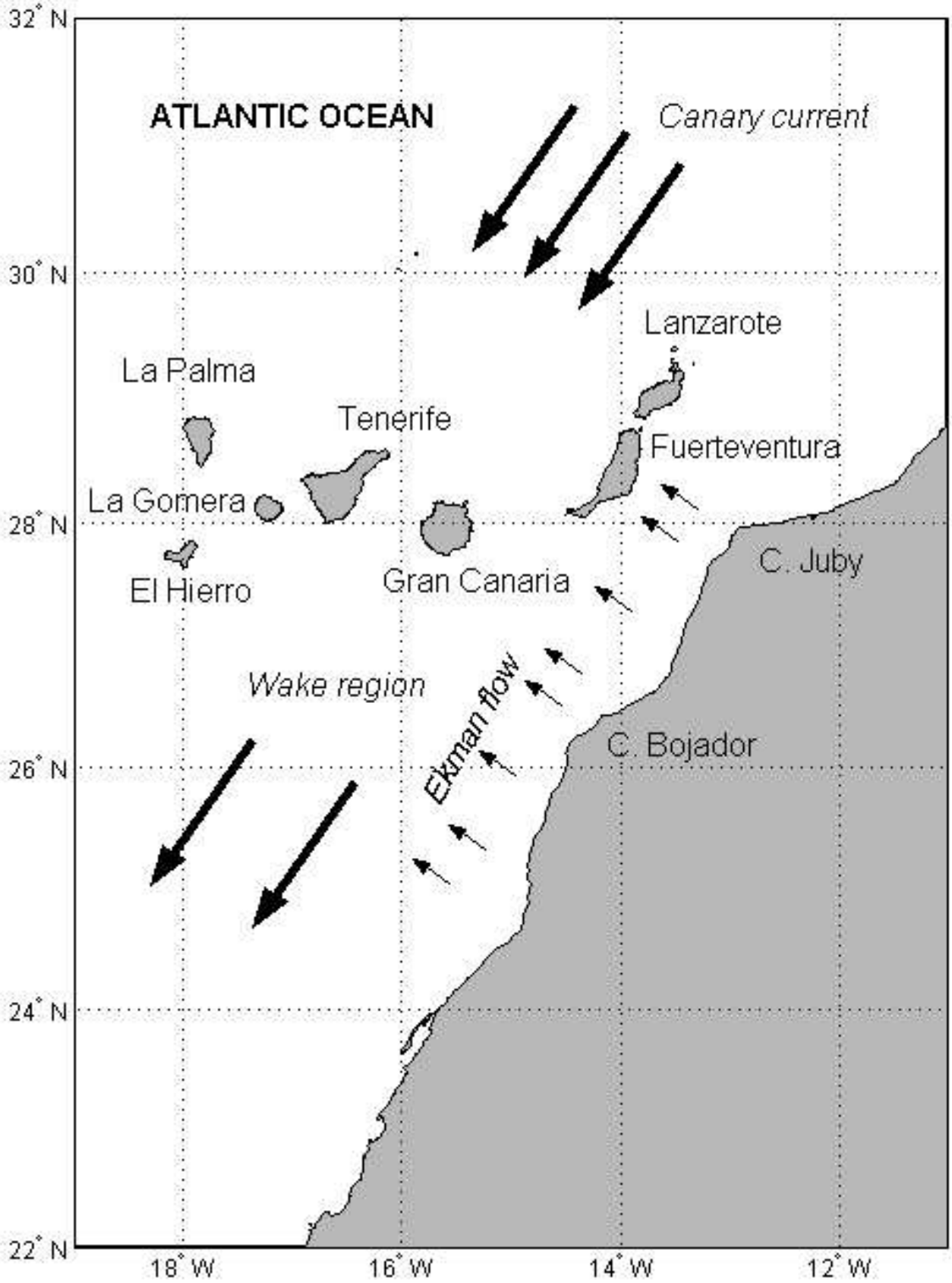

Figure 1. The Canary Islands region, with the Canary current running southwestwards parallel to the African coast, where there is an intense upwelling, and impinging on the islands.

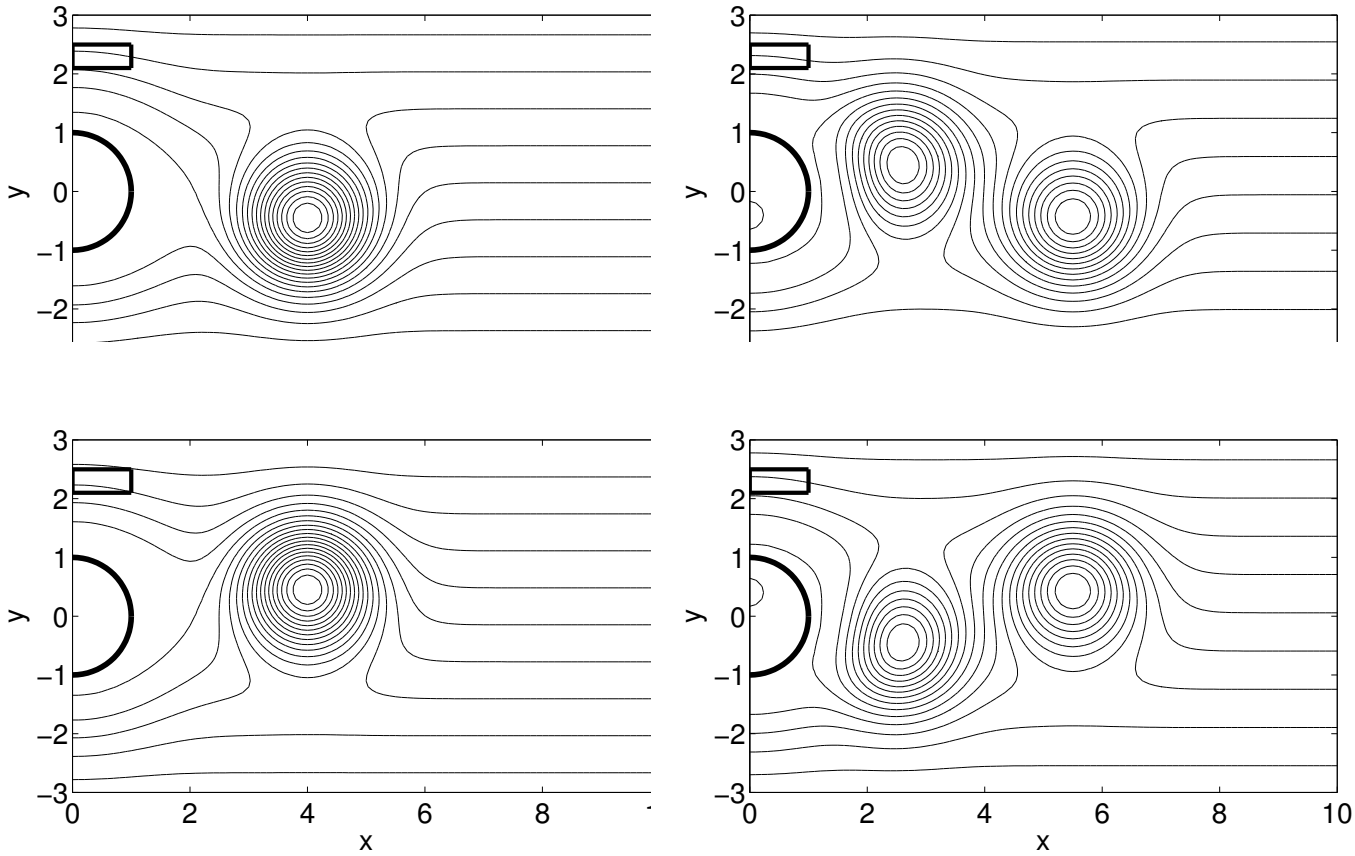

Figure 2. The streamlines of the flow without Ekman flow, $u_E = 0$, at vortex strength $w = 200$. Other parameters as described in Sect. 3. The box where tracers are starting is drawn just above the cylinder with coordinates $0 < x < 1$, and $2.1 < y < 2.5$. The snapshots are at $t = 0$ (top-left), $t = T_c/4$ (top-right), $t = 2T_c/4$ (bottom-left), and $t = 3T_c/4$ (bottom-right).

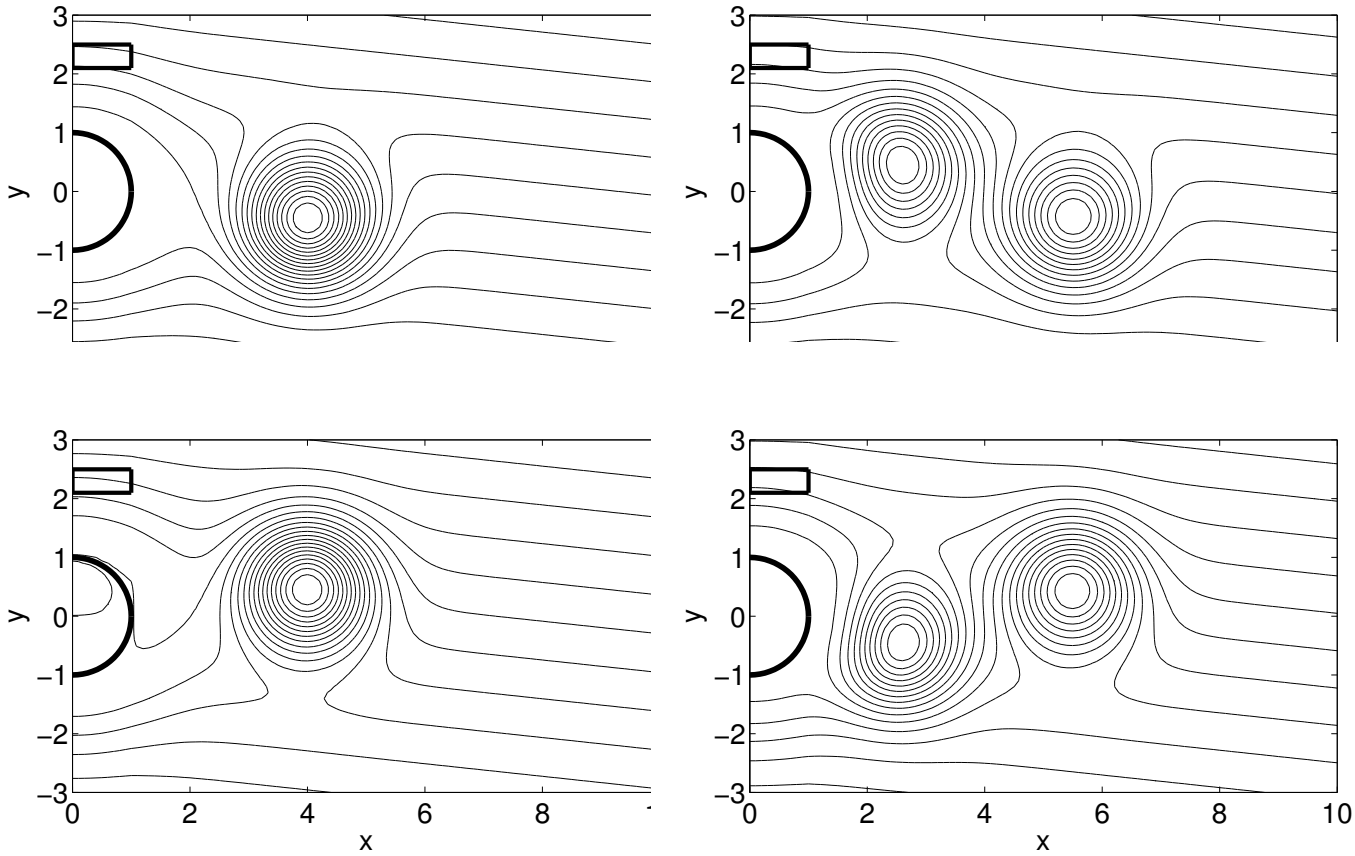

Figure 3. Streamlines of the flow with Ekman flow $u_E = 2$ and other parameters, and time sequence of the snapshots, as in Figure 2.

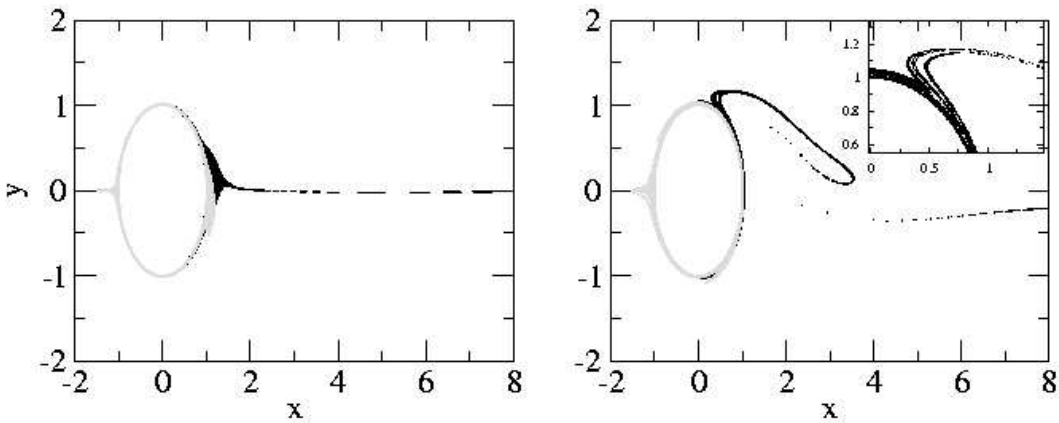

Figure 4. Stable (in gray) and unstable (in black) manifolds of the chaotic saddle in the wake of the cylinder, for the case of the periodic flow and $u_E = 2$. Left: Snapshot taken at time $7T_c$ for vortex strength $w = 10$. Right: Snapshot taken at time $7T_c$ for vortex strength $w = 200$. In the inset we show a zoom of the manifolds in the area close to the cylinder. Other parameters as described in Sect. 3. The chaotic saddle itself is closely packed immediately behind the cylinder surface. The unstable manifold has been plotted by releasing a large number of particles left of the cylinder and very close to it, letting the flow to transport them for a long time ($7T_c$ as already indicated) so that only the ones lasting at this time in the wake region are still there and plotted. The stable manifold is plotted in the same way but releasing the particles right of the cylinder and running the flow backwards in time.

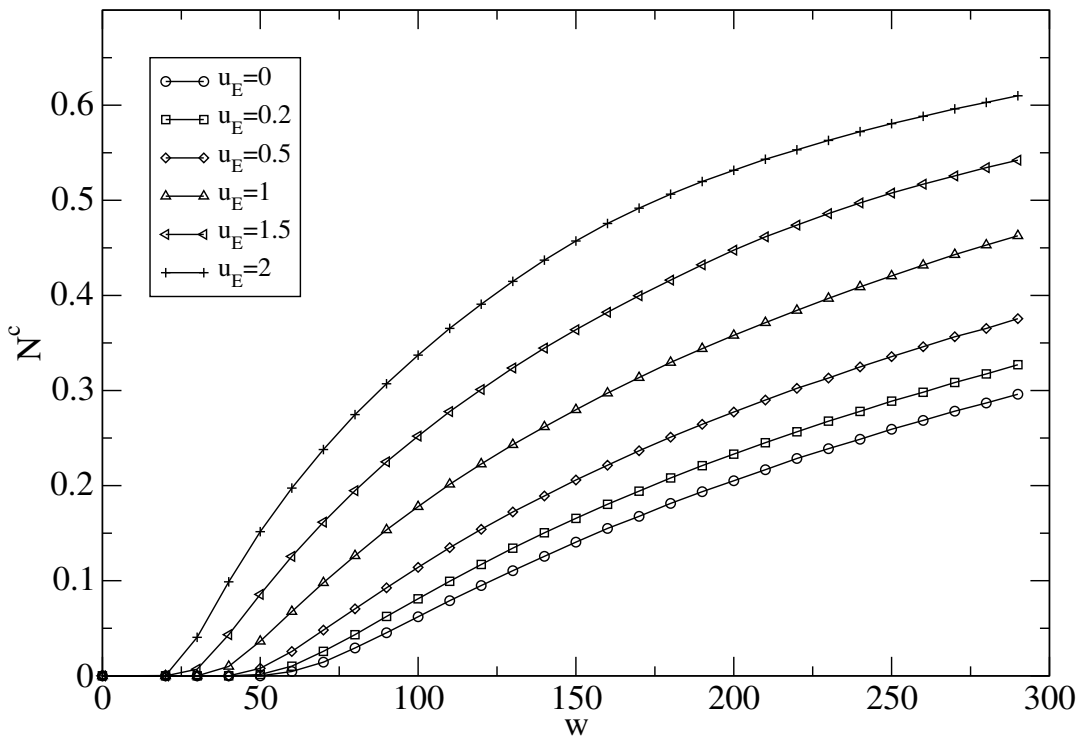

Figure 5. The ratio of particles crossing the wake, N^c, versus vortex strength w in the periodic flow. The different curves correspond to different values of the Ekman pumping, u_E, as indicated in the legend.

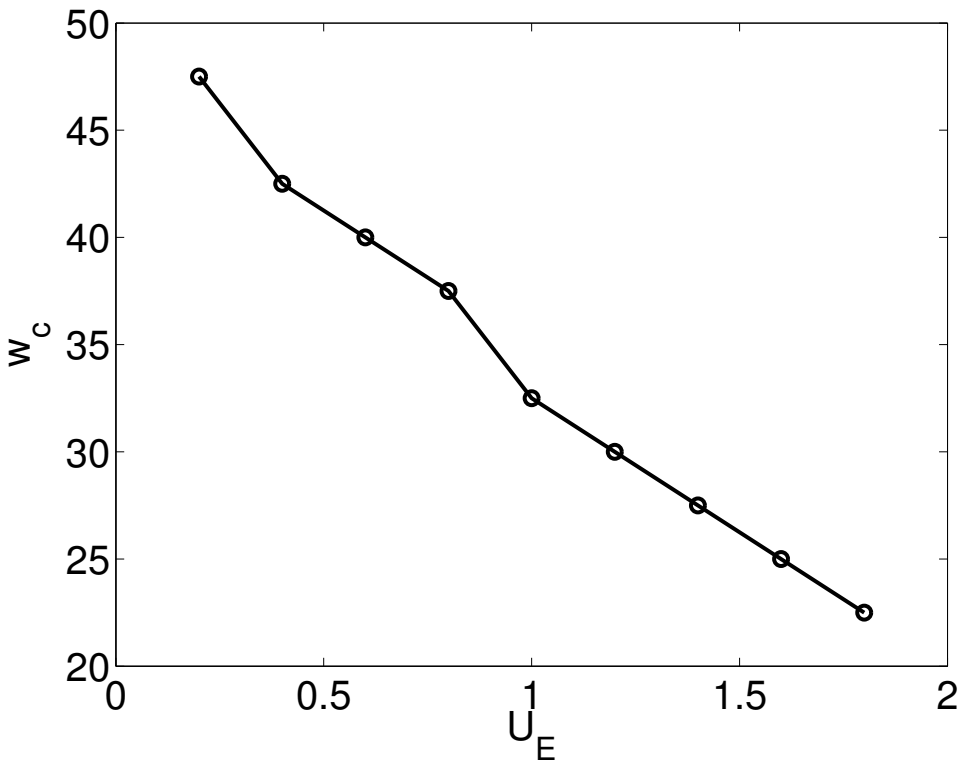

Figure 6. The critical values of the vortex strength, w_c, versus the velocity of the Ekman pumping u_E in the periodic flow.

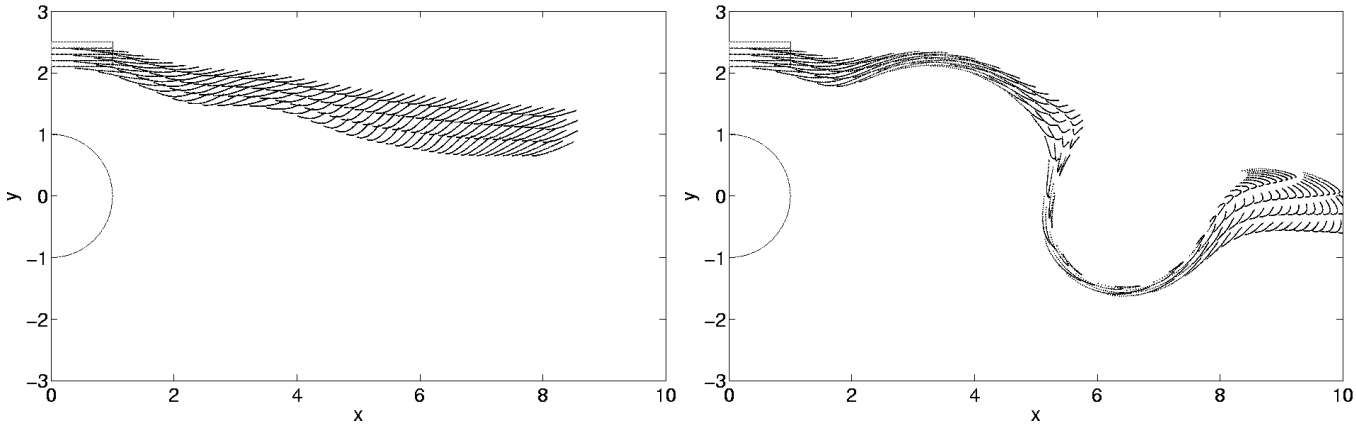

Figure 7. Plot of the spatial distribution of the tracers in the wake of the island for the case of the periodic flow and $u_E = 2$. Left: Snapshot of the distribution of the tracers at time $0.39T_c$ for vortex strength $w = 10$. Right: Snapshot of the distribution of the tracers at time $0.39T_c$ for vortex strength $w = 200$.

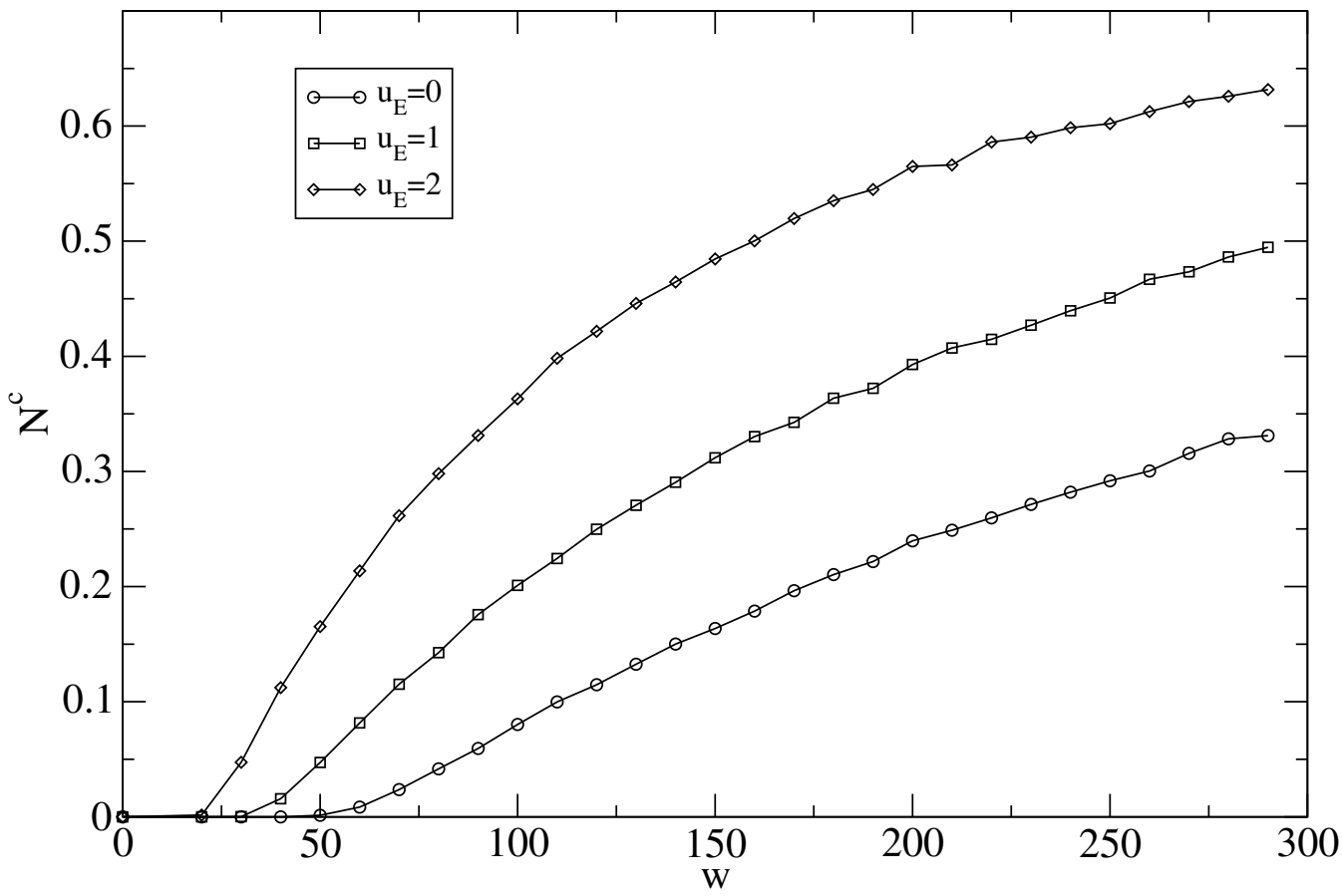

Figure 8. Proportion of particles crossing the wake, N^c, versus vortex strength w for the non-periodic flow. The different curves correspond to different values of the Ekman pumping, u_E, as indicated in the legend.

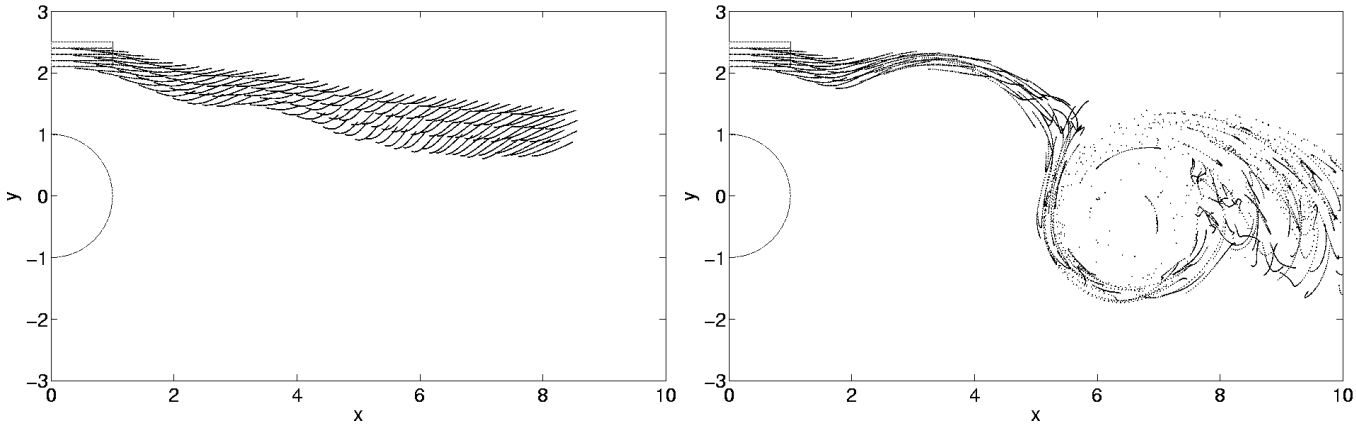

Figure 9. Plot of the spatial distribution of the tracers in the wake of the island for the case of the non-periodic flow and $u_E = 2$. Left: Snapshot of the distribution of the tracers at time $0.39T_c$ for vortex strength $w = 10$. Right: Snapshot of the distribution of the tracers at time $0.39T_c$ for vortex strength $w = 200$.

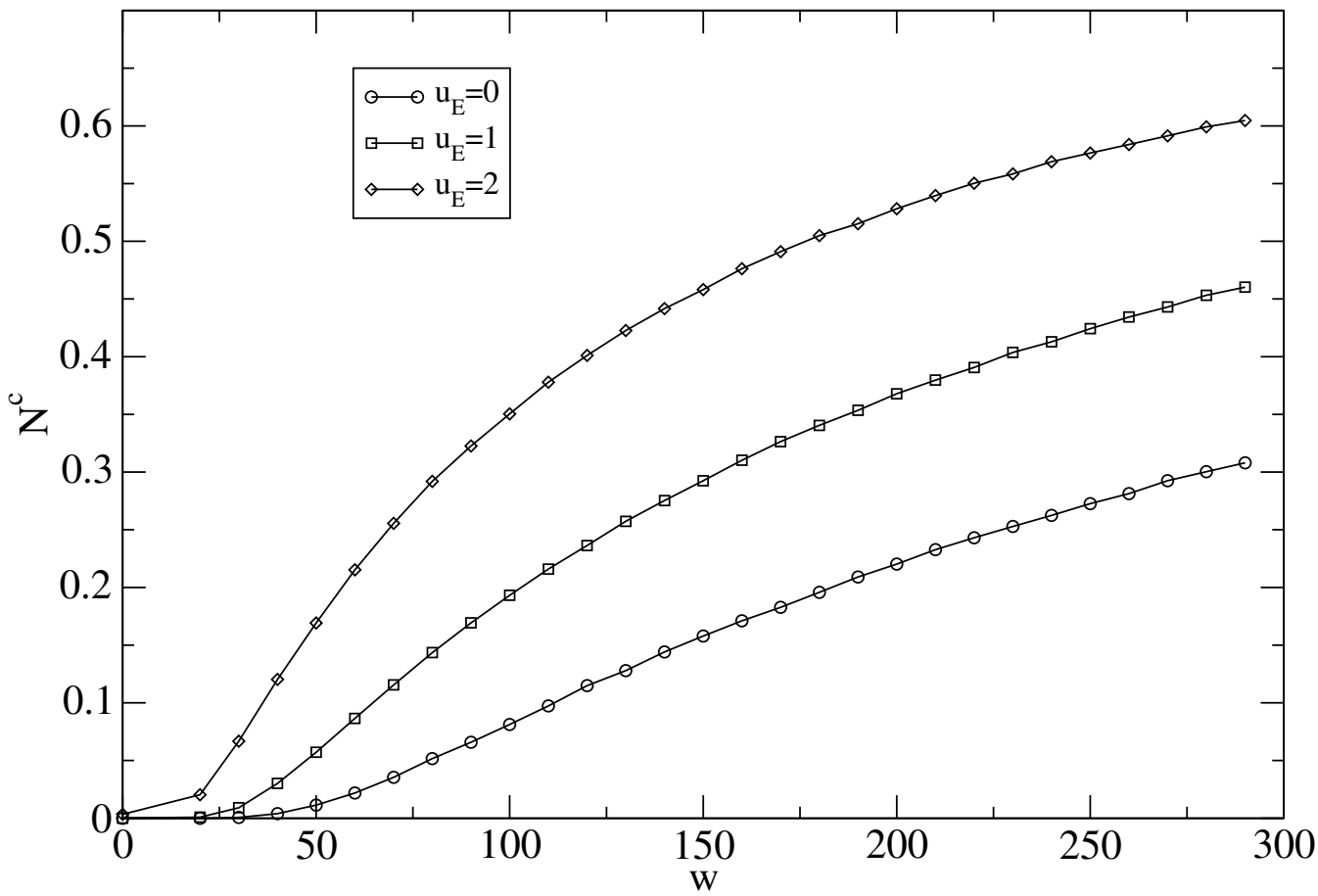

Figure 10. Proportion of particles crossing the wake, N^c, versus vortex strength w for the periodic flow with turbulent diffusion of the particles. The different curves correspond to different values of the Ekman pumping, u_E, as indicated in the legend.

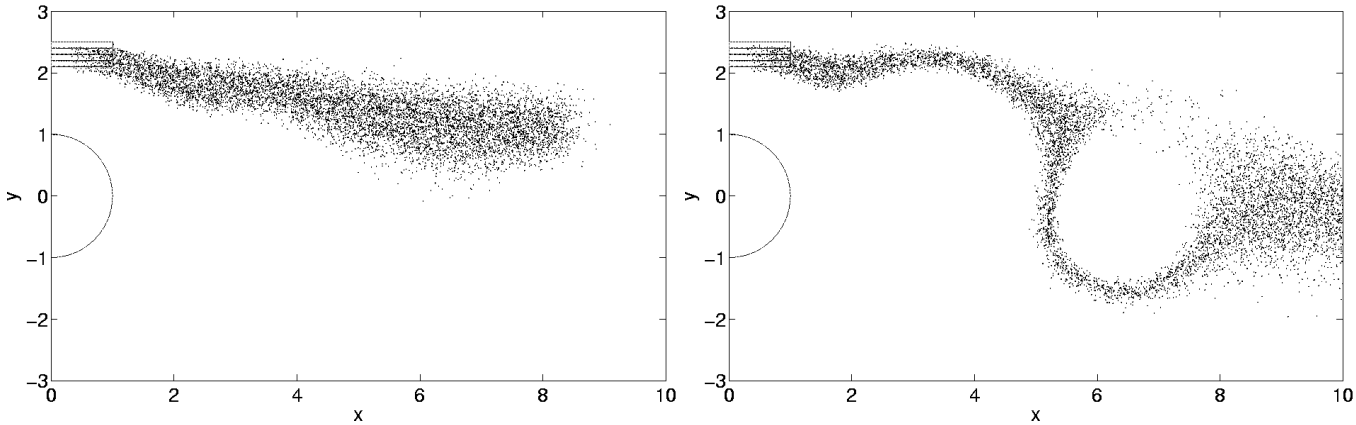

Figure 11. Plot of the spatial distribution of tracers in the wake of the island for the case of the periodic flow with turbulent diffusion and $u_E = 2$. Left: Snapshot of the distribution of the tracers at time $0.39T_c$ for vortex strength $w = 10$. Right: Snapshot of the distribution of the tracers at time $0.39T_c$ for vortex strength $w = 200$.

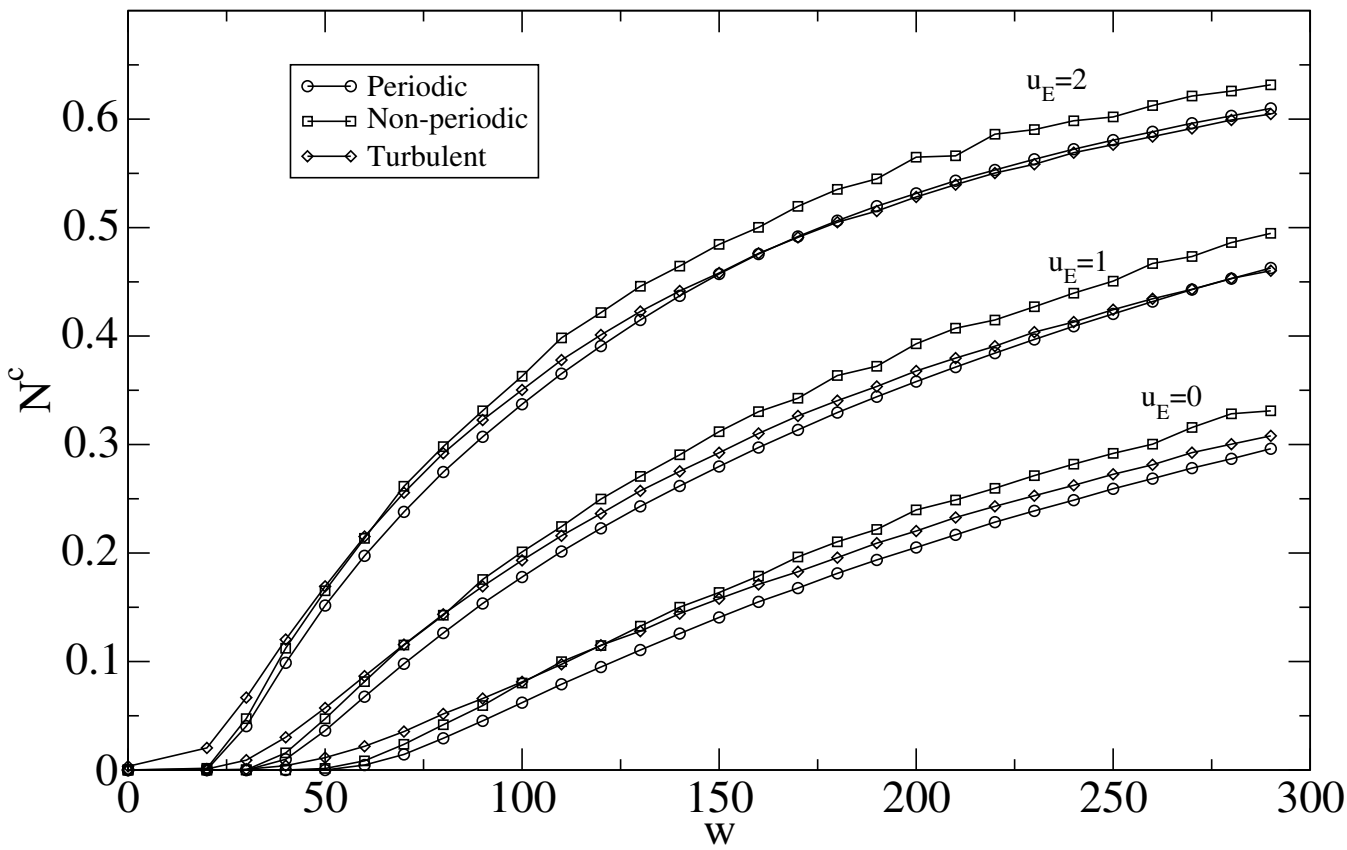

Figure 12. Comparison of transport across the wake for the three kinds of flows. The values of u_E and the type of flow that originated the data are indicated in the plot.

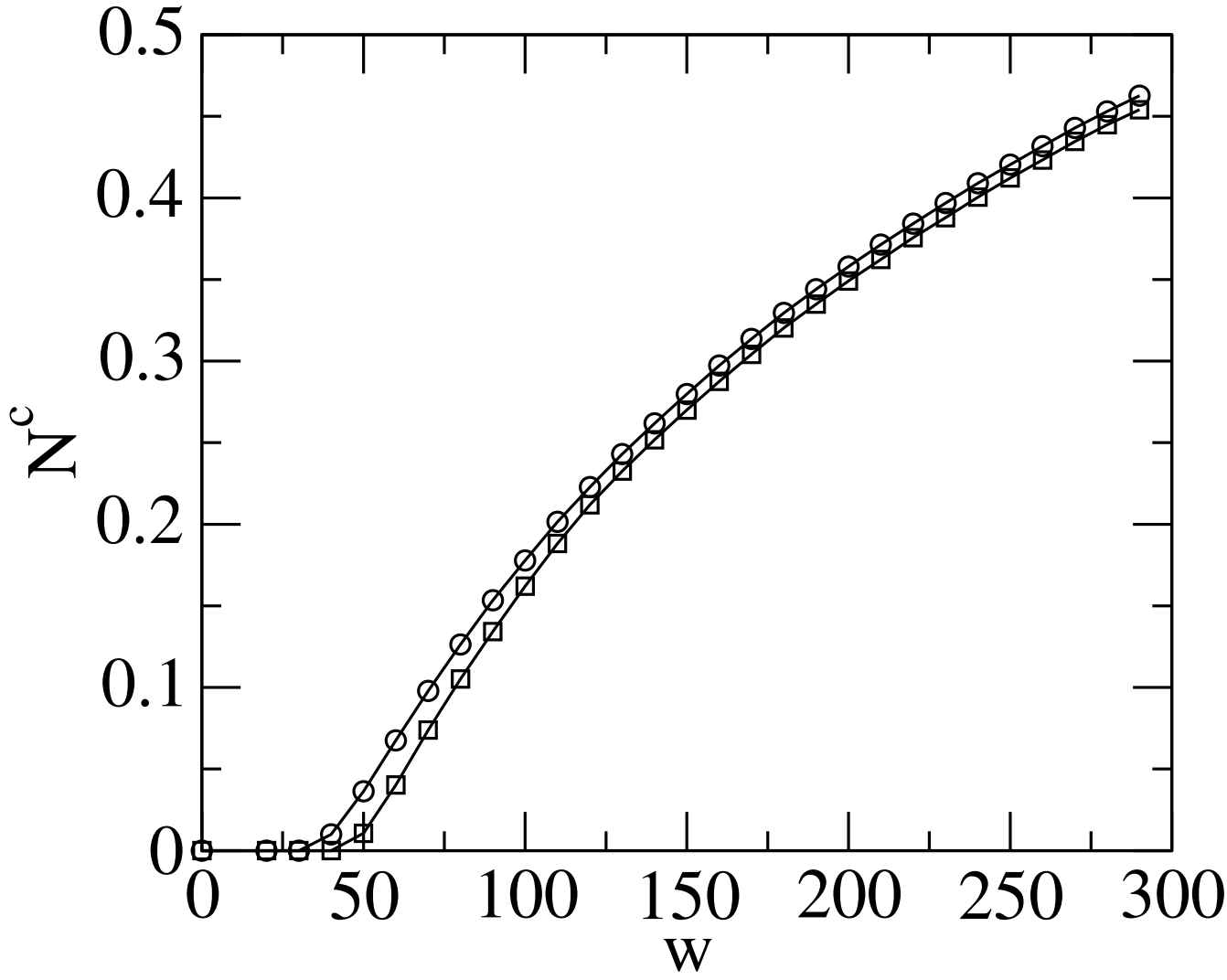

Figure 13. N^c versus w for $u_E = 1$ for the periodic flow, and two situations: circles correspond to the proportion of particles that cross the line $y = 0$, and squares to $y = -1$. No remarkable differences can be observed.